Hexagonally Perforated Layer Morphology in PS-b-P4VP(PDP) Supramolecules

Vukovic, Ivana; ten Brinke, Gerrit; Loos, Katja

Published in:
Macromolecules

DOI:
10.1021/ma301974z

Publication date:
2012

Macromolecules

Article

pubs.acs.org/Macromolecules

Hexagonally Perforated Layer Morphology in PS-*b*-P4VP(PDP) Supramolecules

Ivana Vukovic, Gerrit ten Brinke,* and Katja Loos*

Department of Polymer Chemistry, Zernike Institute for Advanced Materials, University of Groningen, Nijenborgh 4, 9747 AG Groningen, The Netherlands

Supporting Information

ABSTRACT: Supramolecular complexes of polystyrene-*block*-poly(4-vinylpyridine) (PS-*b*-P4VP) diblock copolymers and small molecules such as pentadecylphenol (PDP) have been studied extensively in recent years. In the present study, PS-*b*-P4VP(PDP) complexes with a minority P4VP(PDP) block are morphologically characterized focusing on the region between the lamellar and cylindrical phase. Dynamic mechanical measurements and small-angle X-ray scattering are used to follow the transitions between the ordered states upon heating/cooling. The self-assembled state at various temperatures is determined by small-angle X-ray scattering and transmission electron microscopy. In contrast to the opposite case of majority P4VP(PDP) blocks, where the transition from lamellar to cylindrical structures frequently occurs via the gyroid morphology, the complexes adopt the hexagonally perforated layered morphology in a broad range of compositions. Although known as a metastable phase in pure diblock copolymers, the hexagonally perforated layered phase appears as an equilibrium phase in PS-*b*-P4VP(PDP) complexes, being stabilized by the presence of the hydrogen-bonded PDP side chains in the minority component domains.

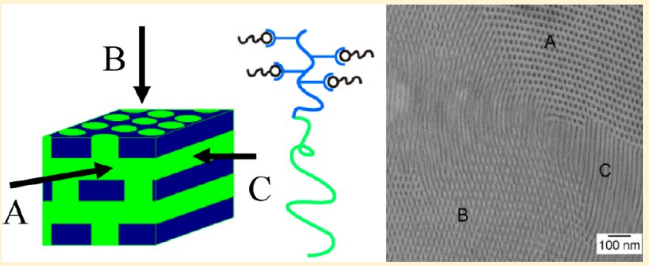

INTRODUCTION

During the last few decades extensive research has been devoted to the field of block copolymers.[1−3] Block copolymers are built out of chemically different blocks that generally repel each other, but their covalent attachment prevents macrophase separation to occur. Instead, microphase separation takes place leading to a variety of ordered nanostructures with ample opportunities for nanotechnological applications.[4−7] Three parameters mainly dictate the phase behavior of block copolymers: (1) the degree of polymerization, N, (2) the Flory−Huggins interaction parameter, χ, and (3) the composition, i.e., the volume fraction of each block, f. A symmetric diblock copolymer (f = 0.5) with sufficiently high χN is ordered into a lamellar structure (LAM). As f increases, the copolymer becomes more asymmetric and morphologies such as cylindrical (CYL) or spherical (SPH) become favorable. In a small part of the phase diagram between the LAM and CYL region, additional intriguing morphologies appear: the gyroid (GYR),[8,9] the hexagonally perforated layers (HPL),[10,11] and the *Fddd* (O^{70}) phase.[12−14] *Fddd* is an orthorhombic, single-network phase, while the GYR phase has a cubic symmetry and consists of two interpenetrated, 3D continuous networks inside a continuous matrix. Besides *Fddd* and GYR morphology, the hexagonally perforated lamellar (HPL) structure has also been found experimentally. The HPL structure consist of alternating layers of the minority and majority component and the former layers contain hexagonally packed cylinders of the majority component. However, theoretical studies found *Fddd* and GYR to be stable equilibrium phases, whereas the HPL is only a metastable phase in neat diblock copolymers.[15,16]

To achieve a specific morphology the system parameters (f, N, χ) have to be selected carefully and this becomes considerably more challenging if the desired structure exists only in a rather narrow range of f and χN values. Additionally, time-consuming elaborate syntheses are required to obtain all the different morphologies in one kind of block copolymer system. The process of creating different morphologies in a given diblock copolymer system can be simplified by adding a component that preferentially resides in the domains of one of the blocks, thereby allowing a simple alteration in the effective composition (f) with concurrent adaptation of the structure. Well-known examples include block copolymer/homopolymer blends in which the homopolymer is chemically identical to one of the copolymer blocks,[17−20] blends in which the homopolymer forms hydrogen bonds with one of the copolymer blocks,[21,22] and mixtures of block copolymers and hydrogen-bonding low molecular weight compounds.[23−26] Their phase behavior often resembles that of neat diblock copolymers. Hashimoto and co-workers studied the phase behavior of polystyrene-*block*-polyisoprene (PS-*b*-PI) blended with polystyrene homopolymer (PS) and found that its phase diagram

Received: September 19, 2012
Revised: November 1, 2012
Published: November 28, 2012

shows complexity and features similar to phase diagrams of pure block copolymers.[20] Shih-Chien Chen et al. investigated blends of poly(4-vinylphenol)-*block*-polystyrene (PVPh-*b*-PS) and homopolymers with different hydrogen bonding strength: poly(4-vinylpyridine) (P4VP), poly(methyl methacrylate) (PMMA), and poly(4-vinylphenol) (PVPh).[22] It was shown that the PVPh-*b*-PS/P4VP blend has a much higher fraction of hydrogen bonded PVPh block compared to the blends with PMMA and PVPh homopolymers. Furthermore, the PVPh-*b*-PS/P4VP blend behaves as a neat diblock copolymer and exhibits the characteristic series of transitions (LAM → GYR → CYL → SPH) as the P4VP content increases.

As segment−segment interaction parameter, χ, is inversely proportional to temperature, the phase behavior of block copolymers is thermally dependent and examples of thermoreversible order−order transitions (OOT) in classical block copolymers, such as cylindrical-to-spherical,[27−29] cylindrical-to-gyroid,[30,31] or lamellar-to-cylindrical,[32,33] have been reported in the literature. In mixtures of block copolymers and hydrogen-bonding low molecular weight compounds, elevated temperatures reduce the strength of hydrogen bonds and may also induce the solubility of low molecular weight compounds in the non-hydrogen bonding block, thus leading to OOTs.[23,24]

Several studies focused on the mixture between polystyrene-*block*-poly(4-vinylpyridine) (PS-*b*-P4VP) copolymer and the low molecular weight amphiphilic compound pentadecylphenol (PDP), that forms hydrogen bonds with the P4VP block.[34,35] Valkama et al. investigated the phase diagram of PS-*b*-P4VP(PDP)$_{1.0}$ (the number in the subscript denotes the ratio between PDP molecules and P4VP monomer units) and, besides classical morphologies, reported novel structures, such as HPL and GYR, in two individual complexes at room temperature (the weight fraction of P4VP(PDP)$_{1.0}$ block, $f_{P4VP(PDP)_x}$, was 0.28 and 0.62, and the total molar mass, including PDP, was 49 500 and 83 300 g mol^{-1}, respectively).[23] In our recent study, the PS-*b*-P4VP(PDP)$_x$ phase behavior in the region between the LAM and CYL phase with P4VP-(PDP)$_x$ being the majority component was meticulously examined.[26] At these compositions the supramolecular complexes appeared to behave very similar to neat diblock copolymers, considering that the transition sequence LAM → GYR → CYL was generally found as the weight fraction of the P4VP(PDP)$_x$ block increased. A set of gyroid samples with tailored feature sizes was obtained in the composition range $0.59 < f_{P4VP(PDP)_x} < 0.65$ and they could be exploited in a number of practical applications.[5−7,36,37]

In the present study, we are focusing on the PS-*b*-P4VP(PDP)$_x$ phase behavior in the region between the CYL and LAM phase at the other side of the phase diagram in which PS represents the majority rather than the minority component. Our initial motivation was to find the gyroid morphology with P4VP(PDP)$_x$ being the minority network component. However, instead of GYR, a surprisingly broad region with HPL was found and a quite fascinating phase behavior was discovered. The PS-*b*-P4VP(PDP)$_x$ complexes investigated are prepared from block copolymer precursors with molar masses ranging from 33 700 to 67 000 g mol^{-1}, and the amount x of PDP added is adjusted to achieve $f_{P4VP(PDP)_x}$ between 0.30 and 0.39. Temperature dependent SAXS and dynamic mechanical measurements are conducted to follow thermally induced order−order phase transitions in the samples and determine their morphologies. TEM is employed as an additional technique to further elucidate room temperature and high temperature equilibrium morphologies of PS-*b*-P4VP(PDP)$_x$ complexes. The HPL morphology appears to be the equilibrium morphology in a broad composition range, in contrast to the phase behavior of neat diblock copolymers. This perforated layered structure was experimentally found before, but the authors could not determine whether it was a metastable or an equilibrium structure.[23,38] Self-consistent mean-field theory calculations by Matsen indicated that the HPL phase can be stabilized by the addition of homopolymer to a diblock copolymer at certain compositions due to the relief of packing frustrations.[39,40] This principle may apply even more to the PS-*b*-P4VP(PDP)$_x$ supramolecular side chain complexes, thus explaining the phase behavior observed.

EXPERIMENTAL SECTION

Materials. *sec*-Butyllithium (*s*BuLi, Acros, 1.3 M in cyclohexane) is used without further purification as an initiator in anionic polymerization. Styrene (St, 99%, Acros) is dried over calcium hydride for 24 h and over dibutylmagesium for another 24 h. Finally, it is condensed into a storage ampule and kept at −18 °C under nitrogen atmosphere. 4-Vinylpyridine (4VP, Acros, 95%) is stirred under nitrogen atmosphere over calcium hydride for 24 h at room temperature and condensed into a flask containing freshly cut sodium. When the solution turned yellowish green, it is condensed into an ampule and stored under nitrogen at −18 °C. Tetrahydrofuran (THF, Acros, 99.9%) is first condensed and then reacted with *tert*-butyllithium for 45 min at −78 °C. A yellow color of solution is the indication that the solvent is suitable for anionic polymerization. Afterward the solvent is condensed into the polymerization flask and degassed by three freeze−pump−thaw cycles. LiCl (Aldrich, 99.99 +%) is dried overnight in vacuum at 130 °C. Several other PS-*b*-P4VP copolymers are supplied by Polymer Source Inc. and used as received. Their properties are listed in Table 1. Chloroform (p.a., LAB-SCAN) is used as received. 3-Pentadecylphenol (PDP, 98%, Aldrich) is recrystallized twice from petroleum ether. Methanol is degassed by argon bubbling for several hours at room temperature.

Table 1. Properties of the Diblock Copolymers PS-*b*-P4VP Used in This Study[a]

sample code	M_n(PS), g mol^{-1}	M_n(P4VP), g mol^{-1}	PDI
S4VP−33.7k[b]	27 200	6500	1.07
S4VP−41.0k[c]	33 000	8000	1.10
S4VP−45.6k[c]	40 000	5600	1.09
S4VP−67.0k[c]	50 000	17000	1.13

[a]The number in the sample code denotes the total molar mass of the block copolymer. [b]Synthesized by anionic polymerization. [c]Obtained from Polymer Source Inc.

Synthesis of PS-*b*-P4VP by Anionic Polymerization. The PS-*b*-P4VP diblock copolymer is synthesized by sequential anionic polymerization in THF at −78 °C on a high-vacuum line. LiCl is added in 5-fold excess relative to the amount of initiator in order to stabilize anionic species and minimize side reactions. Using degassed syringes, St and *s*BuLi are added to the polymerization flask and the reaction is started. After 45 min, a 10 mL sample for GPC analysis is withdrawn and dispersed into degassed methanol. Then the calculated amount of 4VP is added and the reaction is allowed to proceed for another 45 min. The polymerization is terminated by the addition of 5 mL of degassed methanol. The block polymer is precipitated in water and characterized with GPC and ^{1}H NMR. The properties of the synthesized polymer are given in Table 1.

Preparation of the Polymer Films. Films of the supramolecular complexes are cast by dissolving the appropriate amounts of PS-*b*-P4VP diblock copolymer and PDP in chloroform. The concentration of polymer is maintained below 2 wt % to ensure homogeneous

complex formation, and the solution is stirred for a couple of hours at room temperature. Afterward, the solution is poured into a glass Petri dish, which is subsequently placed into a saturated chloroform atmosphere. Chloroform is allowed to evaporate slowly during several days at room temperature. Subsequently, the samples are dried in vacuum at 30 °C overnight and heated for 30 min in an oven at 130 °C.

Characterization. ^{1}H NMR spectra in $CDCl_3$ are recorded on a 400 MHz Varian VXR operating at room temperature.

Gel permeation chromatography (GPC) is performed in DMF (1 mL min^{-1}) with 0.01 M LiBr on a Viscotek GPCmax equipped with model 302 TDA detectors, using two columns (PSS-Gram-1000/30, 10 μ 30 cm). The GPC is calibrated using narrow disperse poly(methyl methacrylate) standards (Polymer Laboratories).

Transmission Electron Microscopy (TEM) is performed on a Philips CM12 transmission electron microscope operating at an accelerating voltage of 120 kV. Images are recorded on a Gatan slow-scan CCD camera. A piece of the film is embedded in epoxy resin (Epofix, Electron Microscopy Sciences) and cured overnight at 40 °C. The sample is subsequently microtomed to a thickness of about 80 nm using a Leica Ultracut UCT-ultramicrotome and a Diatome diamond knife at room temperature. The microtomed sections are floated on water and subsequently placed on copper grids. To obtain contrast for TEM, the samples are stained with iodine (45 min). To study high temperature structures, the samples are first annealed for 4h hours at desired temperature and then quenched in liquid nitrogen.

Small-angle X-ray scattering (SAXS) is performed at the Dutch–Belgian Beamline (DUBBLE) station BM26B of the European Synchrotron Radiation Facility (ESRF) in Grenoble (France). The sample to detector distance is ca. 6 m with a wavelength of 1.033 Å. A Dectris-Pilatus 1 M detector with a resolution of 981 × 1043 pixels and a pixel size of 172 × 172 μm is employed to record the 2D–SAXS scattering patterns. Standard corrections for sample absorption and background subtraction are performed. The data are normalized with respect to the incident beam intensity in order to correct for primary beam intensity fluctuations. The scattering patterns from rat tail are used for the calibration of the wave vector scale of the scattering curve. The SAXS patterns are collected in temperature range between 20 and 200 °C with a heating/cooling rate of 10 °C/min. The scattering vector q is defined as $q = 4\pi/\lambda(\sin\theta)$ with 2θ being the scattering angle.[41,42]

Dynamic mechanical experiments are performed on a AR 1000 N rheometer using an aluminum cone-and-plate fixture of 4° and 20 mm in diameter. The frequency of 0.1 Hz and the strain amplitude of 0.1% are applied to the sample during heating and cooling cycles. Sample temperature is varied in a range between 100 and 200 °C with a heating/cooling rate of 1 °C/min.

RESULTS AND DISCUSSION

To thoroughly explore the phase behavior of PS-*b*-P4VP(PDP)$_x$ complexes, the molar mass of the block copolymer precursors and the amount of PDP in the samples are systematically changed.

We start with a set of PS-*b*-P4VP(PDP)$_x$ complexes prepared from the block copolymer S4VP–33.7k synthesized by living anionic polymerization. The PDP content is varied from $x = 0.3$ to $x = 0.5$, which implies a change in the weight fraction of the P4VP(PDP)$_x$ block from 0.31 to 0.37. Surprisingly, at room temperature all the investigated samples adopt the HPL structure, which subsequently transforms to the CYL phase at higher temperatures. The morphological characterization of a representative sample ($x = 0.5$) is given in Figures 1, 2 and 3. The change in morphology of a block copolymer system can be followed by monitoring the change in its mechanical properties.[43–45] Figure 1 presents the dynamic storage modulus G' during temperature scans of the aforementioned sample at a constant frequency of 0.1 Hz and a constant shear amplitude of 0.1%. G' decreases constantly as the temperature increases to 140 °C and then it suddenly begins to increase indicating a transition between two ordered states. The cooling scan confirms that the observed transition is reversible and that the low temperature phase is thermodynamically stable. To identify the symmetry of both phases, SAXS measurements are performed (Figure 2). SAXS results during cooling (Figure 2a) and heating (Figure 2b) confirm that the reversible order–order transition occurs between 140 and 160 °C. The SAXS intensity pattern of the sample at 200 °C is shown in Figure 2c. The diffraction peaks positioned in the q ratio $1:\sqrt{3}:\sqrt{4}:\sqrt{7}:\sqrt{9}$ indicate the CYL morphology of the complex at high temperatures ($q^* = 0.272$ nm^{-1}, hence, the distance between the cylinders is 26.7 nm). The SAXS curve of the low temperature phase (Figure 2d) contains three peaks at q^*, $1.08q^*$, and $2q^*$, which can be attributed to the HPL structure.[44,46–48] The peak at $0.92q^*$, characteristic for the HPL phase, is comprised in the intense first order diffraction peak and it is not distinguished probably due to the lack of the long-range order. To confirm the low temperature structure of the sample, TEM is employed as a supplementary technique. The schematic representation of the HPL morphology and its various projections is depicted in Figure 3a,c–e) and a good agreement with the experimental TEM data (Figure 3b) is found. In the TEM micrograph, the HPL structure is clearly manifested by the projections parallel (region A and C) and normal (region B) to the perforated layers. The PS domains appear bright while the P4VP(PDP)$_{0.5}$ domains appear dark due to selective iodine staining. The parallel projections consist of alternating layers of majority PS and minority P4VP(PDP)$_{0.5}$ component and the latter are shown with (region A) and without the perforations (region C). Hexagonally packed bright spots result from the normal projection of the PS perforations (region B). The complexes with $x = 0.3$ and $x = 0.4$ exhibit similar phase behaviors (Supporting Information, Figures S1–S4); at room temperature, they adopt the HPL structure which is transformed into the CYL phase as the temperature increases.

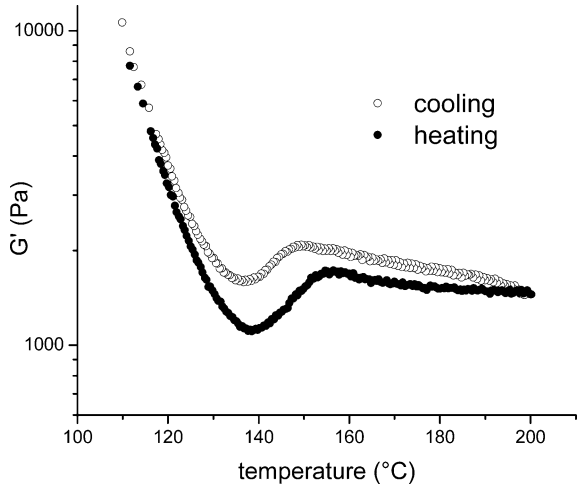

Figure 1. Temperature dependence of the dynamic storage modulus (G') for PS-*b*-P4VP(PDP)$_{0.5}$, $f_{P4VP(PDP)} = 0.37$, $M_{total} = 43\,100$ g mol^{-1} based on S4VP–33.7k. The frequency of shearing is 0.1 Hz, the strain amplitude 0.1%, and the heating/cooling rate is 1 °C/min.

The stability of the HPL phase over a broad composition range may come as a surprise considering the fact that HPL is not an equilibrium structure for neat diblock copolymers. Furthermore, not a single PS-*b*-P4VP(PDP)$_x$ sample from the

dx.doi.org/10.1021/ma301974z | Macromolecules 2012, 45, 9409–9418

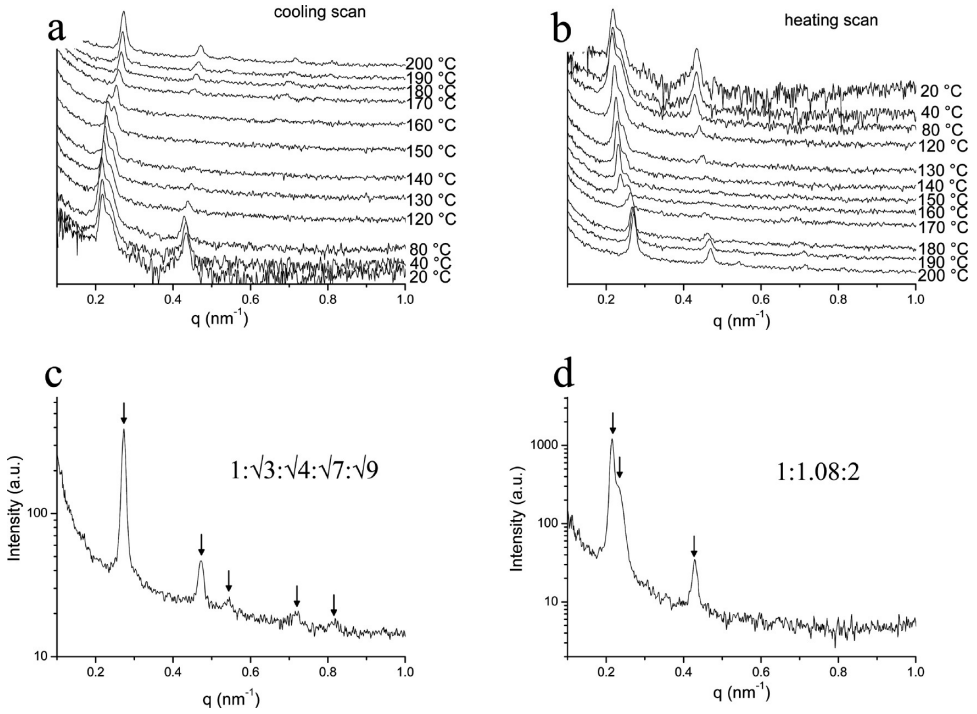

Figure 2. SAXS intensity patterns for PS-*b*-P4VP(PDP)$_{0.5}$, $f_{P4VP(PDP)}$ = 0.37, M_{total} = 43 100 g mol^{-1} based on S4VP−33.7k: (a) as a function of temperature, the sample is cooled from 200 to 20 °C with a cooling rate of 10 °C/min, (b) as a function of temperature, the sample is heated from 20 to 200 °C with a heating rate of 10 °C/min, (c) at 200 °C, and (d) at 80 °C.

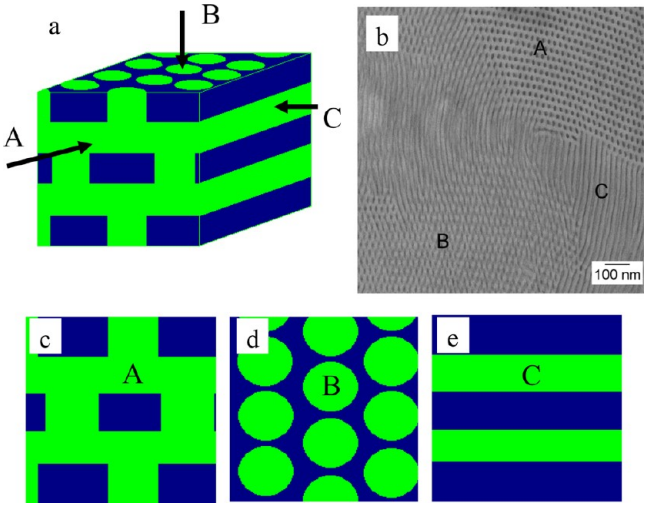

Figure 3. Schematic representation of (a) the HPL morphology, (c) projection parallel to the perforated layers shown with perforations, (d) projection normal to the perforated layers, and (e) projection parallel to the perforated layers shown without perforations; (b) TEM micrograph of PS-*b*-P4VP(PDP)$_{0.5}$, $f_{P4VP(PDP)}$ = 0.37, M_{total} = 43 100 g mol^{-1} based on S4VP−33.7k. The sample acquires the HPL structure at room temperature and the letters A, B, and C denote different projections through the HPL unit cell.

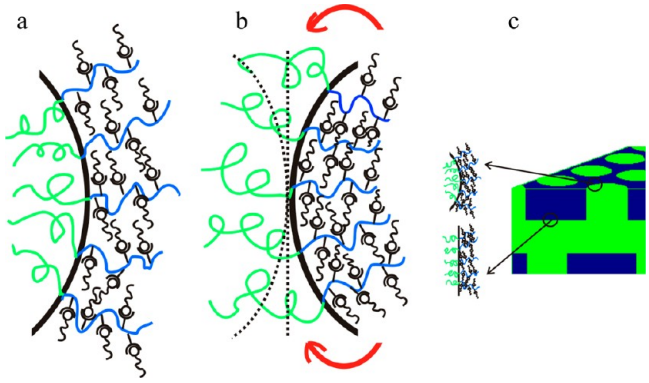

Figure 4. Schematic representation of the situation when (a) P4VP(PDP)$_x$ block represents a majority component in the complex and this situation is favorable; (b) P4VP(PDP)$_x$ block represents a minority component in the complex. This situation is unfavorable and the complexes will tend to either straighten or bend the interfaces to the other side. The HPL structure is atypical since its interfaces are straight or curved with the minority block on the convex side (c).

opposite side of the phase diagram, where P4VP(PDP)$_x$ represents the majority component, adopts the HPL morphology at room temperature.[26] This unique behavior can, however, be explained by the specific supramolecular nature of the PS-*b*-P4VP(PDP)$_x$ complexes. PDP molecules bind to the P4VP monomer units and occupy the space around the P4VP chain forcing it to adopt more stretched conformations. PDP molecules present near the interface between PS and P4VP(PDP)$_x$ can push block copolymer chains from each other, thus increasing the distance between the junction points. This further results in a tendency of the system to create a curved interface, with P4VP(PDP)$_x$ chains positioned on the convex side. For complexes where P4VP(PDP)$_x$ represents the majority component this can be easily accommodated (Figure 4a). The opposite situation, i.e., the formation of the structures in which P4VP(PDP)$_x$ chains are located on the concave side of the interface, is, naturally, unfavorable (Figure 4b). Hence, PS-*b*-P4VP(PDP)$_x$ complexes with $f_{P4VP(PDP)} < 0.5$ will rather form a straight interface than a curved interface with P4VP(PDP)$_x$ blocks on the concave side. This explains the observed asymmetry in the PS-*b*-P4VP(PDP)$_{1.0}$ phase diagram (the

dx.doi.org/10.1021/ma301974z | *Macromolecules* 2012, 45, 9409−9418

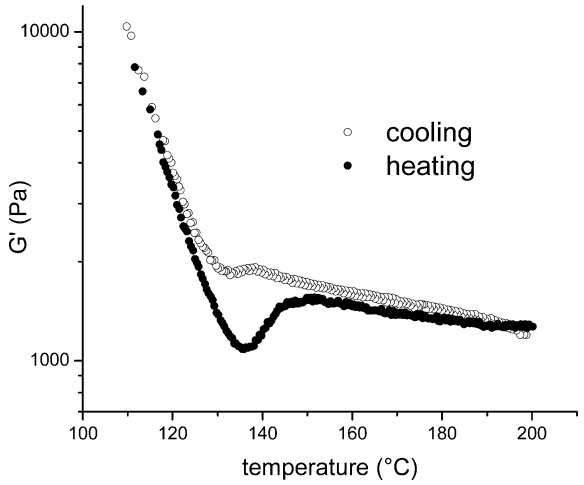

Figure 5. Temperature dependence of the dynamic storage modulus (G') for PS-*b*-P4VP(PDP)$_{0.5}$, $f_{P4VP(PDP)}$ = 0.37, M_{total} = 52 600 g mol^{-1} based on S4VP−41.0k. The frequency of shearing is 0.1 Hz, the strain amplitude is 0.1%, and the heating/cooling rate is 1 °C/min.

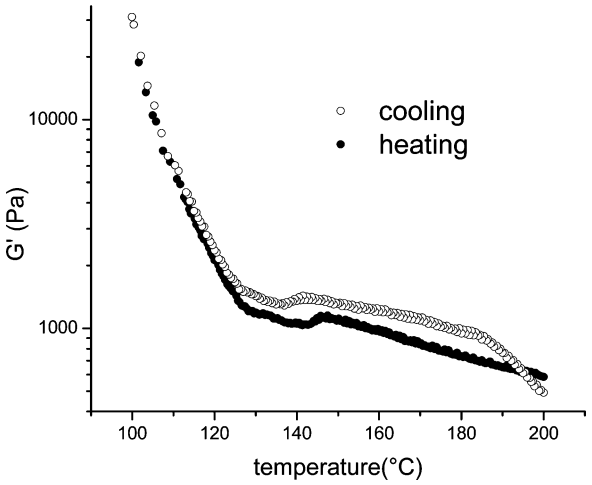

Figure 7. Temperature dependence of the dynamic storage modulus (G') for PS-*b*-P4VP(PDP)$_{1.0}$, $f_{P4VP(PDP)}$ = 0.35, M_{total} = 61 800 g mol^{-1} based on S4VP−45.6k. The frequency of shearing is 0.1 Hz, the strain amplitude 0.1%, and the heating/cooling rate is 1 °C/min.

CYL region is narrower if P4VP(PDP)$_{1.0}$ represents a minority component)[23] or the appearance of the LAM phase in similar supramolecular complexes of polyisoprene-*block*-poly(2-vinylpyridine)(octyl gallate) (PI-*b*-P2VP(OG)) already at $f_{P2VP(OG)}$ = 25.6%.[24] The HPL structure is exceptional because its interfaces are straight or curved in such a manner that the minority component is located on the convex side. This explains why the HPL structure is stabilized in our system and occupies a relatively large composition range (Figure 4c). Theoretical studies demonstrated that in homopolymer/block copolymer blends, the CYL phase is favored when the homopolymer is added to a matrix of the CYL phase since the homopolymer chains fill the corners of Wigner−Seitz cells and relieve the packing frustrations.[39,40] Following a similar

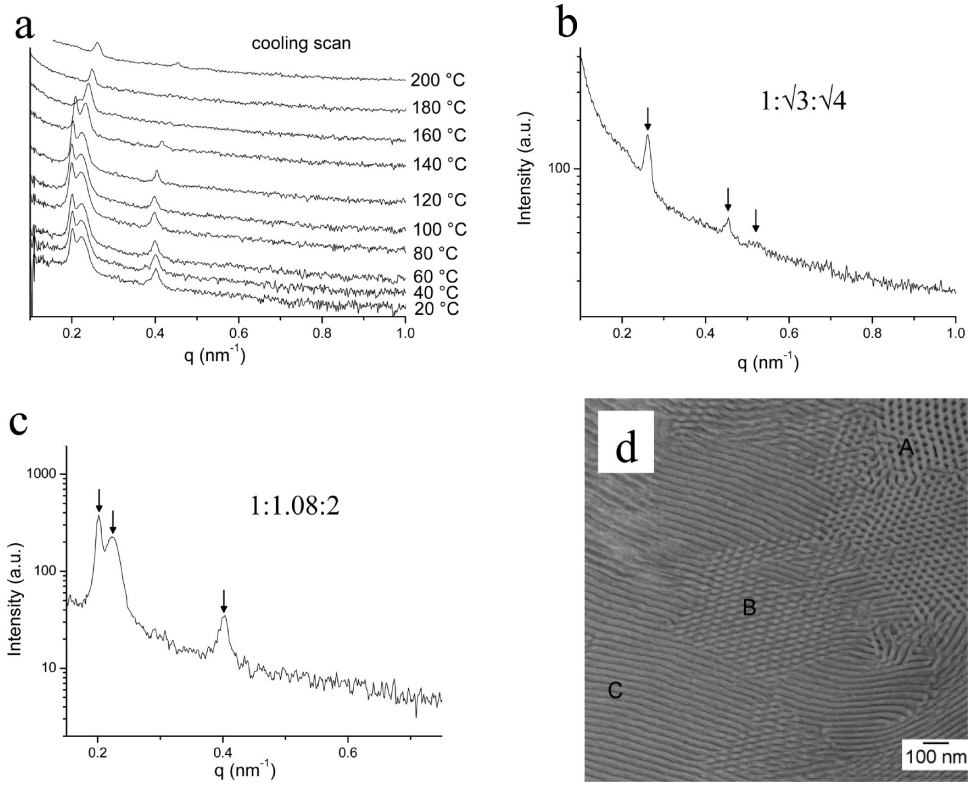

Figure 6. Morphological characterization of PS-*b*-P4VP(PDP)$_{0.5}$, $f_{P4VP(PDP)}$ = 0.37, M_{total} = 52 600 g mol^{-1} based on S4VP−41.0k: (a) SAXS intensity patterns as a function of temperature, the sample is cooled from 200 to 20 °C with a cooling rate of 10 °C/min; (b) SAXS curve at 200 °C. The sample acquires CYL morphology at 200 °C as evidenced by reflections positioned in the relative ratio 1:$\sqrt{3}$:$\sqrt{4}$. (c) SAXS curve at 20 °C indicating the HPL morphology of the sample at room temperature, which is further evidenced by TEM (d). Letters A, B, and C denote different projections through the HPL unit cell.

dx.doi.org/10.1021/ma301974z | *Macromolecules* 2012, 45, 9409−9418

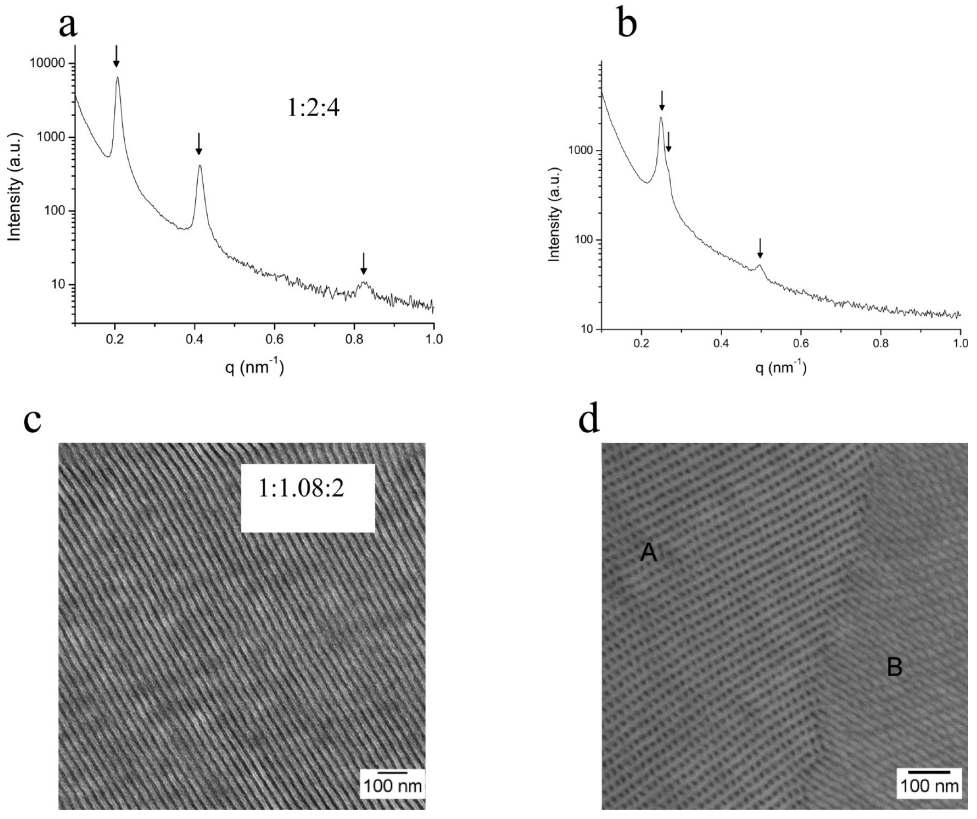

Figure 8. Morphological characterization of PS-*b*-P4VP(PDP)$_{1.0}$, $f_{P4VP(PDP)}$ = 0.35, M_{total} = 61 800 g mol^{-1} based on S4VP−45.6k: (a) SAXS intensity pattern at 20 °C. The sample has LAM morphology at 20 °C, which is also evidenced by TEM (b). At higher temperatures the sample acquires HPL structure, and this is confirmed by SAXS (c) and TEM (d). Letters A and B denote different projections through the HPL unit cell.

mechanism, the HPL phase can be stabilized if the homopolymer is added to a minority component, since in the HPL phase the majority component forms the hexagonally packed channels. Analogously, the presence of PDP in the minority component of PS-*b*-P4VP(PDP)$_x$ complexes may relieve the packing frustrations and stabilize the HPL phase.

FTIR studies show that the strength of the hydrogen bonds in the P4VP(PDP)$_x$ block reduces with heating and, more importantly, PDP becomes soluble in PS above 120 °C.[49] Thus, at higher temperatures a certain amount of PDP migrates to the PS domain inducing a change in the complex composition, i.e., lowering $f_{P4VP(PDP)}$. This explains the order−order transition HPL → CYL observed in the samples based on S4VP−33.7k with x = 0.3−0.5.

To further investigate the phase behavior of PS-*b*-P4VP-(PDP)$_x$ complexes, another sample is prepared from block copolymer S4VP−41.0k with x = 0.5 and $f_{P4VP(PDP)}$ = 0.37. The composition of this sample is identical to the previously described one, but its total molar mass is somewhat higher. Dynamic mechanical measurements indicate the reversible HPL-CYL order−order transition to occur in the range between 130 and 150 °C (Figure 5), which is also confirmed by SAXS during the cooling scan (Figure 6a). At higher temperatures the sample adopts the CYL morphology which is indicated by the SAXS peaks positioned in the ratio 1:$\sqrt{3}$:$\sqrt{4}$ (Figure 6b) with the distance between the cylinders of 27.8 nm (q^* = 0.261 nm^{-1}). The low temperature SAXS pattern (Figure 6c) is similar to the low temperature SAXS pattern of the previously described sample (Figure 2d): three peaks are found at the positions q^*, 1.08q^*, and 2q^* which can be attributed to the HPL phase. The HPL morphology is further confirmed by TEM. Figure 6d depicts different projections through the HPL unit cell: parallel (region A and C) and normal (region B) to the perforated layers. Hence, the HPL morphology encompasses not only a considerable composition range, but it also extends in the vertical (χN) direction in the PS-*b*-P4VP(PDP)$_x$ phase diagram.

Additional TEM images that unambiguously confirm the HPL morphology of the previously described samples are provided in Supporting Information (Figure S5).

The next series of samples is made from the block copolymer S4VP−45.6k with x = 1.0 and 1.2; thus, $f_{P4VP(PDP)}$ = 0.35 and 0.39. These compositions ($f_{P4VP(PDP)}$) are similar to that of the previously described samples, and accordingly, similar phase behavior is expected. Because the ratio between the molar mass of the PS and P4VP block in the block copolymer precursor is higher than in the previous cases, a higher amount of PDP is required to reach the same $f_{P4VP(PDP)}$. This modifies the phase behavior in such a way that at low temperatures now the LAM instead of the HPL phase is found, whereas at higher temperatures the HPL replaces the CYL phase. Figure 7 shows the temperature dependence of G' for the sample based on S4VP−45.6k with x = 1.0 and $f_{P4VP(PDP)}$ = 0.35. The results from the cooling and heating scan imply that the reversible order−order transition takes place between 120 and 150 °C. Below 120 °C the sample has a LAM structure, as confirmed by SAXS (Figure 8a) and TEM (Figure 8b). The SAXS peaks are positioned in the ratio 1:2:4 and the first order reflection appears at q^* = 0.207 nm^{-1} (hence, the lamellar period is 30.3 nm). Above 150 °C, the lamellae are converted into the hexagonally perforated layers, as evidenced by SAXS (Figure 8c) and TEM (Figure 8d). The SAXS reflections at q^*, 1.08q^*,

dx.doi.org/10.1021/ma301974z | *Macromolecules* 2012, 45, 9409−9418

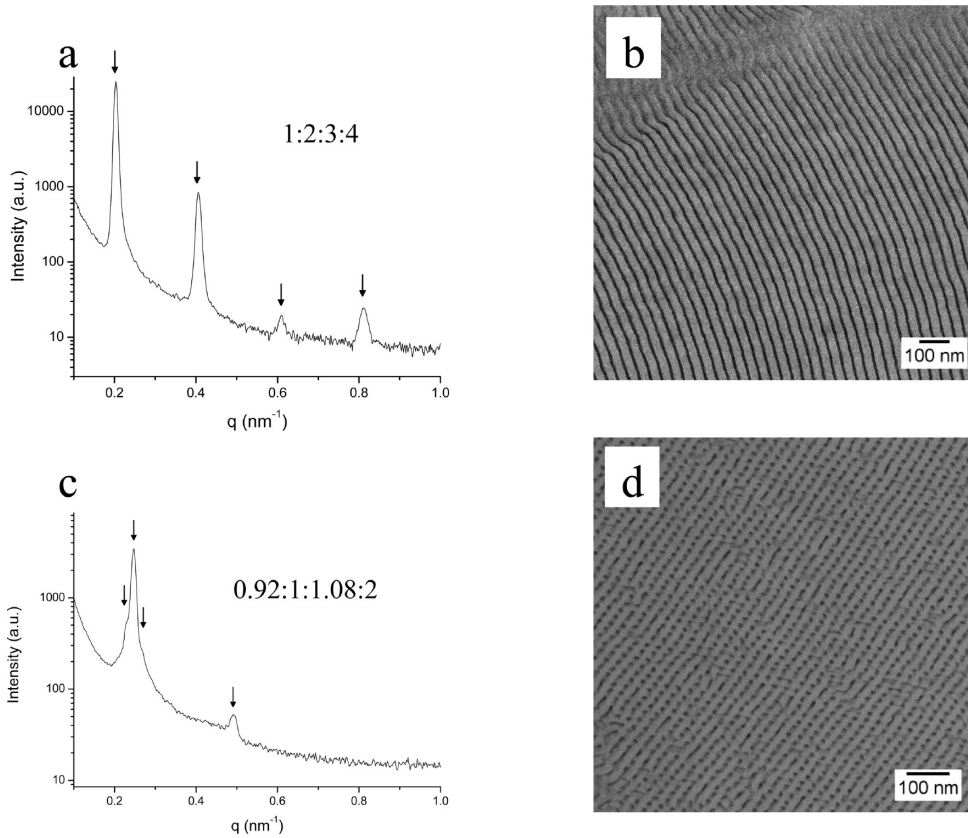

Figure 9. Morphological characterization of PS-*b*-P4VP(PDP)$_{1.2}$, $f_{P4VP(PDP)}$ = 0.39, M_{total} = 65 050 g mol^{-1} based on S4VP−45.6k: (a) SAXS intensity pattern at 20 °C. The sample has LAM morphology at 20 °C, which is also evidenced by TEM (b). At higher temperatures the sample acquires HPL structure, and this is confirmed by SAXS (c) and TEM (d).

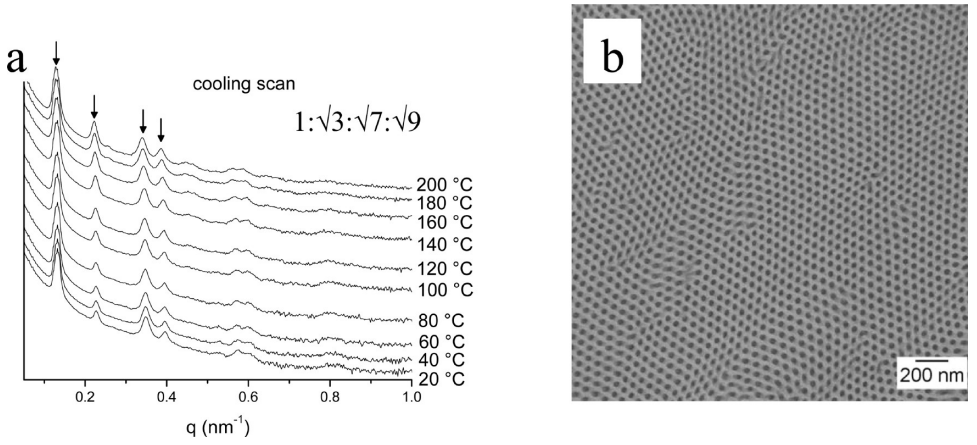

Figure 10. Morphological characterization of PS-*b*-P4VP(PDP)$_{0.1}$, $f_{P4VP(PDP)}$ = 0.30, M_{total} = 71 900 g mol^{-1} based on S4VP−67.0k: (a) SAXS intensity pattern as a function of temperature, the sample is cooled from 200 to 20 °C with a cooling rate of 10 °C/min. In the whole temperature range, the sample exhibits CYL morphology as evidenced by reflections positioned in the relative ratio 1:$\sqrt{3}$:$\sqrt{7}$:$\sqrt{9}$. °C. The CYL morphology of the sample is imaged by TEM (b).

and 2q* indicate the HPL phase while the projections parallel (region A) and normal (region B) to the perforated layers are displayed in the TEM micrograph. Similar phase behavior is found in the complex based on S4VP−45.6k with x = 1.2 and $f_{P4VP(PDP)}$ = 0.39. The low temperature SAXS curve (Figure 9a) contains peaks at q*, 2q*, 3q*, and 4q* demonstrating the LAM structure, which is further confirmed by TEM (Figure 9b). The lamellar period of 30.8 nm follows from q* = 0.204 nm^{-1}. The SAXS pattern of the complex at higher temperatures (Figure 9c) contains the peaks in the ratio 0.92:1:1.08:2 which again is a clear signature of the HPL phase. The alternating layers of the PS and the perforated P4VP domains depicted in the TEM image (Figure 9d) confirm this morphological assignment.

Finally, supramolecular complexes PS-*b*-P4VP(PDP)$_x$ from the block copolymer S4VP−67.0k with x = 0.1, 0.2, and 0.3, hence $f_{P4VP(PDP)}$ = 0.30, 0.35, and 0.39, respectively, are prepared to examine the influence of the molar mass of the block copolymer precursor on the phase behavior of the system. The compositions ($f_{P4VP(PDP)}$) are similar to the

dx.doi.org/10.1021/ma301974z | *Macromolecules* 2012, 45, 9409−9418

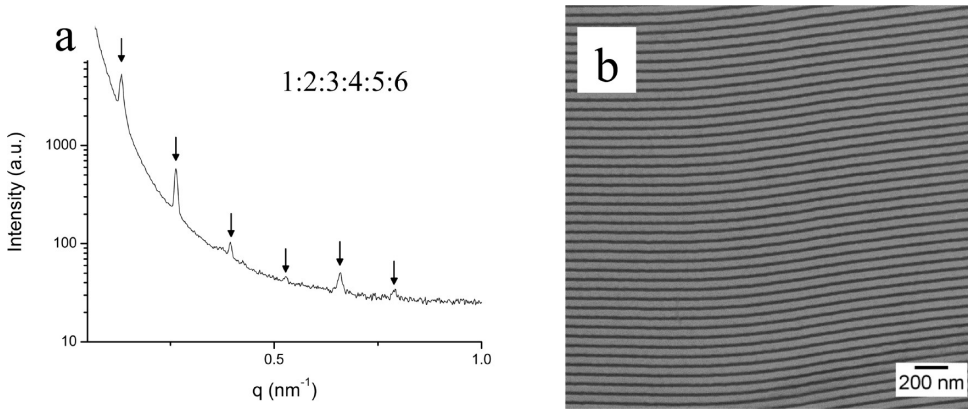

Figure 11. Morphological characterization of PS-*b*-P4VP(PDP)$_{0.3}$, $f_{P4VP(PDP)}$ = 0.39, M_{total} = 81 800 g mol^{-1} based on S4VP−67.0k: (a) SAXS intensity pattern at 180 °C. The sample has a LAM morphology according to SAXS (a) and TEM (b) results.

Table 2. Summary of the Morphological Characterization of Supramolecular Complexes PS-*b*-P4VP(PDP)$_x$

block copolymer code	x	$f_{P4VP(PDP)}$	low T morphology	high T morphology
S4VP−33.7k	0.3	0.31	HPL	CYL
S4VP−33.7k	0.4	0.34	HPL	CYL
S4VP−33.7k	0.5	0.37	HPL	CYL
S4VP−41.0k	0.5	0.37	HPL	CYL
S4VP−45.6k	1.0	0.35	LAM	HPL
S4VP−45.6k	1.2	0.39	LAM	HPL
S4VP−67.0k	0.1	0.30	CYL	CYL
S4VP−67.0k	0.2	0.35	CYL	CYL
S4VP−67.0k	0.3	0.39	LAM	LAM

previously described samples, but the molar mass is somewhat higher. The morphological characterization of the sample with x = 0.1 is given in Figure 10. The diffraction peaks in the SAXS pattern appear at q^*, $\sqrt{3}q^*$, $\sqrt{4}q^*$, and $\sqrt{7}q^*$, which is a clear signature of the CYL phase (Figure 10a). The distance between the cylinders is calculated to be 55.2 nm from q^* = 0.131 nm^{-1}. The SAXS patterns remain identical in the whole temperature range examined and order−order transitions are not observed. This can be understood by realizing that the sample contains very little PDP (x = 0.1) and even if all PDP would migrate completely to the PS domains at elevated temperatures, which is not to be expected, the complex would probably stay inside the CYL region rather than cross over to the SPH region. The TEM micrograph (Figure 10b) shows the P4VP cylinders packed hexagonally in the PS matrix. The sample with x = 0.2 and $f_{P4VP(PDP)}$ = 0.35 exhibits identical phase behavior as the x = 0.1 sample. It also has the CYL morphology in the whole temperature range investigated. When x is increased to 0.3, and accordingly, $f_{P4VP(PDP)}$ to 0.39, the morphology of the supramolecular complex becomes LAM. The diffraction peaks in the SAXS pattern (Figure 11a) at q^*, $2q^*$, $3q^*$, $4q^*$, $5q^*$, and $6q^*$ (lamellar period is calculated to be 47.9 nm) and alternating PS and P4VP(PDP)$_{0.3}$ lamellae shown in the TEM micrograph (Figure 11b) confirm the morphological assignment. This may imply that the HPL phase does not exist in supramolecular complexes PS-*b*-P4VP(PDP)$_x$ if the molar mass of the starting block copolymer exceeds a critical value. On the other hand, it may also be related to the composition of the parent diblock copolymer requiring only a small amount of PDP to reach the composition range of interest. This latter conclusion may well be the most likely one as it is in line with the geometric argument that a curved interface with the minority comb-shaped supramolecular block at the convex side is favored by the comblike molecular architecture (Figure 4c).

The morphological behavior of PS-*b*-P4VP(PDP)$_x$ complexes between the LAM and CYL region with $f_{P4VP(PDP)}$ < 0.5 is summarized in Table 2 and Figure 12.

CONCLUSION

A comprehensive study of the phase behavior of supramolecular complexes PS-*b*-P4VP(PDP)$_x$ with P4VP(PDP)$_x$ as a minority component in the composition range between the CYL and LAM morphology is conducted. Several samples with the HPL structure as equilibrium state have been identified. The HPL phase covers a rather broad composition range. In the set of

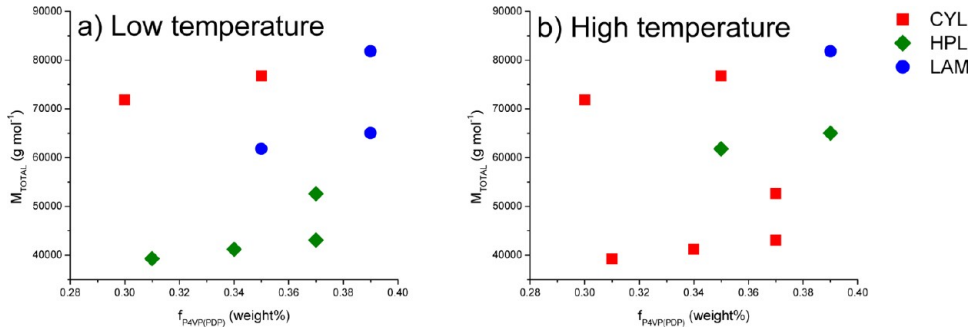

Figure 12. Phase diagram of supramolecular complexes PS-*b*-P4VP(PDP)$_x$ at low (a) and high (b) temperature. The total molar mass of the complex is given at the *y*-axis while the weight fraction of P4VP(PDP) block is given at the *x*-axis.

dx.doi.org/10.1021/ma301974z | *Macromolecules* 2012, 45, 9409−9418

samples prepared from the block copolymer S4VP−33.7k, for instance, it extends from $f_{P4VP(PDP)} = 0.31$ to $f_{P4VP(PDP)} = 0.37$, and presumably even further. This atypical phase behavior can be explained by the presence of PDP "side chain" molecules in the minority component of the complex, where the HPL morphology reliefs the packing frustrations. Several PS-*b*-P4VP(PDP)$_x$ complexes undergo order−order transition upon heating due to composition changes accompanying the migration of part of the PDP to the PS domains at elevated temperatures. Besides the composition, the total molar mass and the amount of PDP(x) is an important factor that determines the phase behavior of the complexes. Finally, the HPL phase spans a considerable χN range, but above a certain value of the molar mass of the starting block copolymer, it seems to disappear from the phase diagram. This study reveals once more the exciting phase behavior of PS-*b*-P4VP(PDP)$_x$ complexes, which provides a powerful tool to design tailor-made structures for numerous practical applications.

■ ASSOCIATED CONTENT

Ⓢ Supporting Information

SAXS intensity patterns and TEM micrographs. This material is available free of charge via the Internet at http://pubs.acs.org.

■ AUTHOR INFORMATION

Corresponding Author

*E-mail: (K.L.) k.u.loos@rug.nl; (G.t.B.) g.ten.brinke@rug.nl.

Notes

The authors declare no competing financial interest.

■ ACKNOWLEDGMENTS

The authors are grateful to Vincent Voet and Martin Faber for their guidance and help with the high vacuum system for anionic polymerization, Joop Vorenkamp for GPC measurements and Gert Alberda van Ekenstein for assistance with dynamic mechanical experiments. Beamtime at DUBBLE (ESRF, Grenoble) has kindly been made available by The Netherlands Organization for Scientific Research (NWO) and we would like to acknowledge Daniel Hermida Merino for experimental assistance and useful discussions.

■ REFERENCES

(1) Bates, F. S.; Fredrickson, G. H. *Annu. Rev. Phys. Chem.* **1990**, *41*, 525−527.

(2) Hamley, I. W., *The Physics of Block Copolymers*. Oxford University Press: Oxford, U.K., 1998.

(3) Abetz, V.; Simon, P. Phase Behaviour and Morphologies of Block Copolymers. In *Adv. Polym. Sci.*: Springer: Berlin/Heidelberg, Germany: 2005; Vol. *189*, pp 125−212.

(4) Hamley, I. W. *Nanotechology* **2003**, *14*, 39−54.

(5) Crossland, E. J. W.; Kamperman, M.; Nedelcu, M.; Ducati, C.; Wiesner, U.; Smilgies, D. M.; Toombes, G. E. S.; Hillmyer, M. A.; Ludwigs, S.; Steiner, U.; Snaith, H. J. *Nano Lett.* **2009**, *9*, 2807−2812.

(6) Vukovic, I.; Punzhin, S.; Vukovic, Z.; Onck, P.; De Hosson, J. T. M.; ten Brinke, G.; Loos, K. *ACS Nano* **2011**, *5*, 6339−6348.

(7) Vignolini, S.; Yufa, N. A.; Cunha, P. S.; Guldin, S.; Rushkin, I.; Stefik, M.; Hur, K.; Wiesner, U.; Baumberg, J. J.; Steiner, U. *Adv. Mater.* **2012**, *24*, OP23−OP27.

(8) Hajduk, D. A.; Harper, P. E.; Gruner, S. M.; Honeker, C. C.; Kim, G.; Thomas, E. L.; Fetters, L. J. *Macromolecules* **1994**, *27*, 4063−4075.

(9) Schulz, M. F.; Bates, F. S.; Almdal, K.; Mortensen, K. *Phys. Rev. Lett.* **1994**, *73*, 86−89.

(10) Hamley, I. W.; Koppi, K. A.; Rosedale, J. H.; Bates, F. S.; Almdal, K.; Mortensen, K. *Macromolecules* **1993**, *26*, 5959−5970.

(11) Foerster, S.; Khandpur, A. K.; Zhao, J.; Bates, F. S.; Hamley, I. W.; Ryan, A. J.; Bras, W. *Macromolecules* **1994**, *27*, 6922−6935.

(12) Tyler, C. A.; Morse, D. C. *Phys. Rev. Lett.* **2005**, *94*, 208302.

(13) Ranjan, A.; Morse, D. C. *Phys Rev E* **2006**, *74*, 011803.

(14) Kim, M. I.; Wakada, T.; Akasaka, S.; Nishitsuji, S.; Saijo, K.; Hasegawa, H.; Ito, K.; Takenaka, M. *Macromolecules* **2008**, *41*, 7667−7670.

(15) Matsen, M. W.; Schick, M. *Phys. Rev. Lett.* **1994**, *72*, 2660−2663.

(16) Laradji, M.; Shi, A.-C.; Noolandi, J.; Desai, R. C. *Macromolecules* **1997**, *30*, 3242−3255.

(17) Tanaka, H.; Hasegawa, H.; Hashimoto, T. *Macromolecules* **1991**, *24*, 240−251.

(18) Mayes, A. M.; Russell, T. P.; Satija, S. K.; Majkrzak, C. F. *Macromolecules* **1992**, *25*, 6523−6531.

(19) Torikai, N.; Takabayashi, N.; Noda, I.; Koizumi, S.; Morii, Y.; Matsushita, Y. *Macromolecules* **1997**, *30*, 5698−5703.

(20) Bodycomb, J.; Yamaguchi, D.; Hashimoto, T. *Macromolecules* **2000**, *33*, 5187−5197.

(21) Dobrosielska, K.; Wakao, S.; Suzuki, J.; Noda, K.; Takano, A.; Matsushita, Y. *Macromolecules* **2009**, *42*, 7098−7102.

(22) Chen, S.-C.; Kuo, S.-W.; Jeng, U. S.; Su, C.-J.; Chang, F.-C. *Macromolecules* **2010**, *43*, 1083−1092.

(23) Valkama, S.; Ruotsalainen, T.; Nykänen, A.; Laiho, A.; Kosonen, H.; ten Brinke, G.; Ikkala, O.; Ruokolainen, J. *Macromolecules* **2006**, *39*, 9327−9336.

(24) Bondzic, S.; Polushkin, E.; Ruokolainen, J.; ten Brinke, G. *Polymer* **2008**, *49*, 2669−2677.

(25) Nandan, B. *J. Polym. Sci., B: Polym. Phys.* **2010**, *48*, 1594−1605.

(26) Vukovic, I.; Voortman, T. P.; Merino, D. H.; Portale, G.; Hiekkataipale, P.; Ruokolainen, J.; ten Brinke, G.; Loos, K. *Macromolecules* **2012**, *45*, 3503−3512.

(27) Sakurai, S.; Kawada, H.; Hashimoto, T.; Fetters, L. J. *Macromolecules* **1993**, *26*, 5796−5802.

(28) Kim, J. K.; Lee, H. H.; Ree, M.; Lee, K.-B.; Park, Y. *Macromol. Chem. Phys.* **1998**, *199*, 641−653.

(29) Krishnamoorti, R.; Modi, M. A.; Tse, M. F.; Wang, H. C. *Macromolecules* **2000**, *33*, 3810−3817.

(30) Wang, C.-Y.; Lodge, T. P. *Macromolecules* **2002**, *35*, 6997−7006.

(31) Lin, S.-H.; Ho, C.-C.; Su, W.-F. *Soft Matter* **2012**, *8*, 4890−4893.

(32) Hajduk, D. A.; Gruner, S. M.; Rangarajan, P.; Register, R. A.; Fetters, L. J.; Honeker, C.; Albalak, R. J.; Thomas, E. L. *Macromolecules* **1994**, *27*, 490−501.

(33) Ryu, D. Y.; Lee, D. H.; Jeong, U.; Yun, S.-H.; Park, S.; Kwon, K.; Sohn, B.-H.; Chang, T.; Kim, J. K.; Russell, T. P. *Macromolecules* **2004**, *37*, 3717−3724.

(34) Mäki-Ontto, R.; de Moel, K.; de Odorico, W.; Ruokolainen, J.; Stamm, M.; ten Brinke, G.; Ikkala, O. *Adv. Mater.* **2001**, *13*, 117−121.

(35) Ikkala, O.; ten Brinke, G. *Science* **2002**, *295*, 2407−2409.

(36) Hsueh, H.-Y.; Chen, H.-Y.; She, M.-S.; Chen, C.-K.; Ho, R.-M.; Gwo, S.; Hasegawa, H.; Thomas, E. L. *Nano Lett.* **2010**, *10*, 4994−5000.

(37) Hsueh, H.-Y.; Ho, R.-M. *Langmuir* **2012**, *28*, 8518−8529.

(38) Ruotsalainen, T.; Turku, J.; Hiekkataipale, P.; Vainio, U.; Serimaa, R.; ten Brinke, G.; Harlin, A.; Ruokolainen, J.; Ikkala, O. *Soft Matter* **2007**, *3*, 978−985.

(39) Matsen, M. W. *Macromolecules* **1995**, *28*, 5765−5773.

(40) Matsen, M. W. *Phys. Rev. Lett.* **1995**, *74*, 4225−4228.

(41) Borsboom, M.; Bras, W.; Cerjak, I.; Detollenaere, D.; Glastra Van Loon, D.; Goedtkindt, P.; Konijnenburg, M.; Lassing, P.; Levine, Y. K.; Munneke, B.; Oversluizen, M.; Van Tol, R.; Vlieg, E. *J. Synchrotron Radiat.* **1998**, *5*, 518−520.

(42) Bras, W.; Dolbnya, I. P.; Detollenaere, D.; van Tol, R.; Malfois, M.; Greaves, G. N.; Ryan, A. J.; Heeley, E. *J. Appl. Crystallogr.* **2003**, *36*, 791−794.

(43) Khandpur, A. K.; Foerster, S.; Bates, F. S.; Hamley, I. W.; Ryan, A. J.; Bras, W.; Almdal, K.; Mortensen, K. *Macromolecules* **1995**, *28*, 8796−8806.

(44) Ahn, J.-H.; Zin, W.-C. *Macromolecules* **2000**, *33*, 641−644.

(45) Ahn, J.-H.; Zin, W.-C. *Macromol. Res.* **2003**, *11*, 152−156.

(46) Ahn, J.-H.; Zin, W.-C. *Macromolecules* **2002**, *35*, 10238−10240.
(47) Lai, C.; Loo, Y.-L.; Register, R. A.; Adamson, D. H. *Macromolecules* **2005**, *38*, 7098−7104.
(48) Hajduk, D. A.; Takenouchi, H.; Hillmyer, M. A.; Bates, F. S.; Vigild, M. E.; Almdal, K. *Macromolecules* **1997**, *30*, 3788−3795.
(49) Ruokolainen, J.; Saariaho, M.; Ikkala, O.; ten Brinke, G.; Thomas, E. L.; Torkkeli, M.; Serimaa, R. *Macromolecules* **1999**, *32*, 1152−1158.